Soil Dynamics and Earthquake Engineering 29 (2009) 765–781

Contents lists available at ScienceDirect

Soil Dynamics and Earthquake Engineering

journal homepage: www.elsevier.com/locate/soildyn

Macroelement modeling of shallow foundations

C.T. Chatzigogos [a,b,*], A. Pecker, J. Salençon [a,b]

[a] Solid Mechanics Laboratory CNRS UMR 7649, Department of Mechanics, École Polytechnique, Palaiseau 91128 Cedex, France
[b] Geodynamique et Structure 157 rue des Blains 92220 Bagneux France

ARTICLE INFO

Article history:
Received 31 October 2007
Received in revised form
12 July 2008
Accepted 19 August 2008

Keywords:
Shallow foundations
Displacement-based design
Non-linear dynamic analysis
Plasticity
Uplift

ABSTRACT

The paper presents a new macroelement model for shallow foundations. The model is defined through a non-linear constitutive law written in terms of some generalized force and displacement parameters. The linear part of this constitutive law comes from the dynamic impedances of the foundation. The non-linear part comprises of two mechanisms. One is due to the irreversible elastoplastic soil behavior. It is described with a bounding surface hypoplastic model, adapted for the description of the cyclic soil response. An original feature of the formulation is that the bounding surface is considered independently of the surface of ultimate loads of the system. The second mechanism concerns the detachment that can take place at the soil–footing interface (foundation uplift). It is totally reversible and non-dissipative and can thus be described by a phenomenological non-linear elastic model. The macroelement model is qualitatively validated by application to soil–structure interaction analyses of simple real structures and by comparison with results from more sophisticated methods of analysis.

1. Introduction

1.1. Definition of the "macroelement"

We are presenting in this paper a new formulation for the modeling of shallow foundations of structures using the concept of macroelement. The macroelement can be viewed as a practical tool that allows for efficient dynamic analyses of structures with consideration of non-linear soil–structure interaction effects arising at the foundation level. As a generic example, we consider the configuration in Fig. 1, in which a soil–foundation–superstructure system is subjected to a dynamic excitation at the bedrock denoted by $\ddot{u}$. The problem viewed in its entirety entails a number of non-linearities such as the irreversible elastoplastic soil behavior and the unilateral soil–foundation interface conditions leading to uplift of structures. These non-linearities render the numerical treatment of the problem within a classical finite-element framework delicate and particularly expensive. Furthermore, the dynamic nature of the problem makes it even more challenging. The model needs to be able to accommodate for an accurate description of the wave propagation and radiation phenomena (the second arise as waves emanate from the foundation towards infinite extremities of the soil medium) and it is clear that fully non-linear dynamic analyses in the time domain for three-dimensional configurations remain beyond the reach of conventional computational capacities. In such a setting, the concept of "macroelement" is introduced by replacing the entire foundation–soil system by a single element that is placed at the base of the superstructure and aims at reproducing the non-linear soil–structure interaction effects taking place at the foundation level. Consequently, this element exhibits a non-linear "constitutive law", which links some generalized force parameters to the corresponding kinematic ones. The generalized force and displacement parameters are chosen in such a way so as to be coherent with those adopted for the superstructure model.

1.2. Existing macroelement models for shallow foundations

The concept of "macroelement" was initially introduced in the context of shallow foundations by Nova and Montrasio [1]. Based on a number of experimental tests performed on a perfectly rigid strip footing resting on a frictional soil and subjected to an eccentric and inclined force, Nova and Montrasio formulated a global elastoplastic model with isotropic hardening for the entire soil–foundation system. The model was written in terms of resultant vertical and horizontal forces and moment acting on the footing normalized by the maximum supported vertical force and was used for the prediction of the footing displacements for quasistatic monotonic loading. The rugby-ball-shaped *surface of ultimate loads* of the system was identified as the *yield surface* of the plasticity model. This surface is schematically presented in Fig. 2.

The model of Nova and Montrasio was first modified by Paolucci [2] for application to structures subjected to real dynamic loading and further extended by Pedretti [3] for a more accurate

* Corresponding author.
E-mail addresses: charisis.chatzigogos@lmsgc.enpc.fr, charisis.chatzigogos@wanadoo.fr, charisis.chatzigogos@geodynamique.com (C.T. Chatzigogos).

0267-7261/$ - see front matter © 2008 Elsevier Ltd. All rights reserved.
doi:10.1016/j.soildyn.2008.08.009

Nomenclature

Latin

a	characteristic dimension of strip or circular footing
A	footing area (or area/length for strip footing)
B	width of strip footing
c_0, ∇c	soil cohesion at the surface of the ground, vertical cohesion gradient
d	depth of soil layer
C_{ij}, $i, j = N, V, M$	imaginary part of dynamic impedances of foundation (radiation damping)
C_S	structural damping coefficient
D	diameter of circular footing
$f_{BS}(\underline{Q})$	analytical expression of bounding surface in the space of generalized forces
$\mathscr{G}$	elastic shear modulus of the soil
h	scalar quantity used for the definition of the plastic modulus
h_0	numerical parameter used for the definition of the scalar quantity h
H	height (of a superstructure)
$\underline{\underline{\mathscr{H}}}$	(normalized) generalized plastic modulus
$\mathbf{I(P)}$	image point on the bounding surface of a point $\mathbf{P}$
J_F	mass moment of inertia of the foundation
$\mathscr{K}_{ij}$, $i, j = N, V, M$	normalized elements of the elastic stiffness matrix
$\tilde{\mathscr{K}}_{ij}$, $i, j = N, V, M$	normalized static impedances of the foundation
K_{ij}, $i, j = N, V, M$	dimensional elements of the elastic stiffness matrix
$\tilde{\mathscr{K}}_{ij}$, $i, j = N, V, M$	dimensional static impedances of the foundation
K_S	dimensional structural stiffness
L	length of strip footing
m_S, m_F	mass of the superstructure, mass of the foundation
M	moment applied on the footing
N	vertical force applied on the footing
N_c	bearing capacity coefficient
N_{max}	maximum centered vertical force supported by the footing
$\underline{n}$	unit normal vector on the bounding surface
p_1	parameter of the plasticity model—plastic response in reloading
q	surface surcharge
q_i, $i = N, V, M$	normalized cinematic parameters of macroelements
q_u, q_u°	ultimate pressure below strip and circular footing
$\underline{q}$	vector of normalized cinematic parameters of macroelements
$\dot{\underline{q}}^{el}$, $\dot{\underline{q}}^{pl}$	increments of elastic and plastic parts of the vector of cinematic parameters
$q^{el}_{M,0}$	elastic normalized rotation angle at the moment of uplift initiation
Q_i, $i = N, V, M$	normalized force parameters of macroelements
$\underline{Q}$	vector of normalized force parameters of macroelements
$Q_{M,0}$	normalized uplift initiation moment
$Q_{V,max}$, $Q_{M,max}$	parameters used for the definition of the bounding surface
V	horizontal force on the footing
V_{La}	Lysmer's analog velocity
V_S	shear wave velocity
$\underline{u}, \dot{\underline{u}}, \ddot{\underline{u}}$	displacement, velocity and acceleration field
$\mathscr{W}$	normalized work of external forces
W	dimensional work of external forces
x, y, z	Cartesian coordinates

Greek

α, β	uplift parameters: definition of moment of uplift initiation
θ	rotation angle
λ	measure of the distance between current stress point and its image point
λ_{min}	minimum attained value for the quantity λ during the loading history
μ_c, ν_c	parameters in the bearing capacity solutions presented in [34]
ν	Poisson's ratio
ρ	soil mass density
σ, τ	normal, tangential traction on an interface

description of the system behavior under cyclic loading. Crémer [4] and Crémer et al. [5,6] presented an advanced macroelement model with the coupling of two separate mechanisms: the first one refers to the material non-linearity of the system due to the irreversible elastoplastic soil behavior and the second one describes the uplift of the footing due to unilateral contact

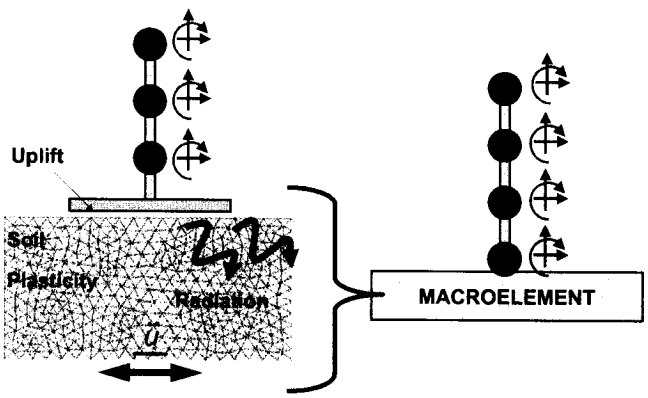

Fig. 1. Generic soil–foundation–structure system subjected to dynamic loading and macroelement concept.

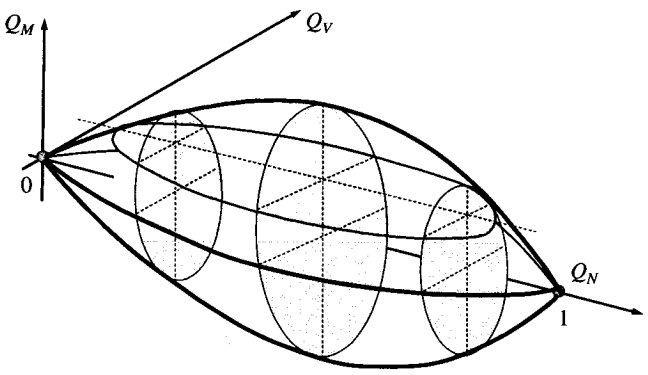

Fig. 2. Rugby-ball-shaped surface of ultimate loads identified as the yield surface of the plasticity model in the model of Nova and Montrasio [1] and its evolution models.

Table 1
Overview of existing macroelement models for shallow foundations

Reference	Year	Configuration	Description
Nova and Montrasio	1991	Strip footing resting on a purely frictional soil	Isotropic hardening plasticity model and non-associated flow rule. Application in the case of quasistatic monotonic loading
Paolucci	1997	Strip footing resting on a purely frictional soil	Perfect plasticity model with non-associated flow rule. Application to simple structures subject to seismic loading. Parametric studies
Pedretti	1998	Strip footing resting on a purely frictional soil	Hypoplastic model for the description of the system response under cyclic loading. Consideration of uplift by reduction of elastic stiffness. Applications to structures subject to quasistatic cyclic loading
Gottardi et al. [12]	1999	Strip footing resting on a purely frictional soil	Isotropic hardening plasticity model. Detailed description of the system ultimate surface (identified as the yield surface of the plasticity model) via "swipe tests". Application in the case of quasistatic monotonic loading
Le Pape et al. Le Pape and Sieffert	1999 2001	Strip footing resting on a purely frictional soil	Elastoplastic model derived from thermodynamical principles. Rugby-ball-shaped yield surface and ellipsoidal plastic potential. Application to seismic loading
Crémer et al.	2001, 2002	Strip footing resting on a purely cohesive soil without resistance to tension	Non-associated plasticity model with isotropic and kinematic hardening coupled with a model for uplift. Application to seismic loading
Martin and Houlsby [13]	2001	Circular footing resting on a purely cohesive soil	Non-associated plasticity model with isotropic hardening. Detailed description of the yield surface via "swipe tests". Application to quasistatic monotonic loading
Houlsby and Calssidy [14]	2002	Circular footing resting on a purely frictional soil	Non-associated plasticity model with isotropic hardening. Detailed description of the yield surface via "swipe tests". Application to quasistatic monotonic loading
Di Prisco et al. [15]	2003	Strip footing resting on a purely frictional soil	Hypoplastic model for the description of the behavior under cyclic loading. Application to quasistatic cyclic loading
Cassidy et al. [16]	2004	Circular footing resting on a frictional or cohesive soil	Fully three-dimensional formulation. Application to the off-shore industry. Quasistatic monotonic loading
Houlsby et al.	2005	Strip or circular footing resting on cohesive soil. Frictional soil–footing interface	Decoupled Winkler springs with elastic perfectly plastic contact-breaking law derived from thermodynamical principles. Application to quasistatic cyclic loading
Einav and Cassidy	2005	Strip footing resting on cohesive soil. Frictional soil–footing interface	Decoupled Winkler springs with elastoplastic contact-breaking law with hardening derived from thermodynamical principles. Application to quasistatic cyclic loading
Grange et al. (*cf.* [17])	2006	Circular footing on cohesive soil	Extension of the plasticity model of Crémer to purely three-dimensional setting. No separate uplift model included

conditions along the interface. For the description of the system behavior under cyclic loading, Crémer formulated a plasticity model with isotropic and kinematic hardening. Le Pape et al. [7] and Le Pape and Sieffert [8] presented a macroelement model similar to the one proposed by Nova and Montrasio particularly oriented towards earthquake engineering applications and based on thermodynamical principles. Several macroelement models have also been proposed in the context of off-shore foundation design for a variety of soil conditions and foundation geometries [13,14,16]. Efforts have been made to obtain global models of shallow foundations by considering uncoupled Winkler springs attached at the foundation interface as in [9,10] that are characterized by an elastoplastic contact-breaking law. The advantage of such formulations is that they permit derivation of the global system response by integration of the local spring response, which can be achieved analytically. On the other hand, they are subject to certain limitations associated with the Winkler decoupling hypothesis, such as the difficulty to calibrate model parameters. Finally we note that the concept of macroelement has been applied to other types of geotechnical problems such as the dynamic response of gravity walls (*cf.* [11]). The non-exhaustive Table 1 presents an overview of some existing macroelement models for shallow foundations.

2. Model formulation

2.1. Definition of generalized forces and displacements

The modeling procedure is initiated with the definition of generalized forces and displacements, in terms of which "constitutive" equations for macroelements are written. We will present in the following the proposed model for two particular cases of footing geometry: (a) a perfectly rigid strip footing of width B and (b) a perfectly rigid circular footing of diameter D. In both cases the footing is supposed to rest at the surface of the ground. So the embedment depth is zero. The perfect rigidity of the footing determines the movement of all its points as soon as the movement of a single point is known. We thus consider the resultant forces in the vertical and horizontal direction and the resultant moment acting at the center of the footing. We also consider the corresponding kinematic parameters: vertical and horizontal displacements and angle of rotation at the center of the footing. For the case of circular footing, a planar loading will be considered in the following as being more relevant to earthquake loading conditions and in order to facilitate comparisons with the case of strip footing. The examined footing together with the considered generalized forces and displacements is presented in Fig. 3.

The "constitutive" equations of the macroelement will be written in terms of the force and displacement parameters presented in Fig. 3, normalized according to the following scheme:

$$\underline{Q} = \begin{pmatrix} Q_N \\ Q_V \\ Q_M \end{pmatrix} = \begin{pmatrix} N/N_{\max} \\ V/N_{\max} \\ M/aN_{\max} \end{pmatrix}, \quad \underline{q} = \begin{pmatrix} q_N \\ q_V \\ q_M \end{pmatrix} = \begin{pmatrix} u_z/a \\ u_x/a \\ \theta_y \end{pmatrix} \tag{1}$$

In (1), $a = B$ and D for a strip and a circular footing, respectively, and $N_{\max}$ is the maximum centered vertical force supported by the footing, i.e. in the absence of any horizontal force and moment. From now on, $N_{\max}$ will always refer to this quantity. The introduced normalization leads to the following expression

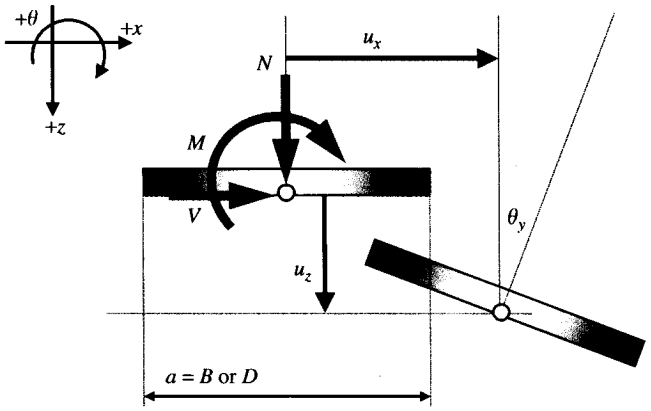

Fig. 3. Definition of generalized forces and displacements for a perfectly rigid footing under planar loading.

for the work of the force parameters:

$$\mathscr{W}(\underline{Q},\underline{q}) = \underline{Q}\cdot\underline{q} = \frac{1}{aN_{\max}}(Nu_z + Vu_x + M\theta_y) = \frac{W}{aN_{\max}} \tag{2}$$

where the total work W in the system is normalized by the characteristic quantity $aN_{\max}$. We also note that if the force and displacement increments are related to each other by the introduction of a general stiffness matrix as in the following expression:

$$\begin{pmatrix}\dot{Q}_N\\ \dot{Q}_V\\ \dot{Q}_M\end{pmatrix} = \begin{bmatrix}\mathscr{K}_{NN} & \mathscr{K}_{NV} & \mathscr{K}_{NM}\\ \mathscr{K}_{VN} & \mathscr{K}_{VV} & \mathscr{K}_{VM}\\ \mathscr{K}_{MN} & \mathscr{K}_{MV} & \mathscr{K}_{MM}\end{bmatrix}\begin{pmatrix}\dot{q}_N\\ \dot{q}_V\\ \dot{q}_M\end{pmatrix} \tag{3}$$

then, following (1), the elements of the stiffness matrix are subjected to the following normalization scheme:

$$\underline{\underline{\mathscr{K}}} = \frac{1}{N_{\max}}\begin{bmatrix}aK_{NN} & aK_{NV} & K_{NM}\\ aK_{VN} & aK_{VV} & K_{VM}\\ K_{MN} & K_{MV} & \frac{1}{a}K_{MM}\end{bmatrix} \tag{4}$$

The quantities $\mathscr{K}_{ij}$, $i,j = N, V, M$ in (3) represent normalized elements of the stiffness matrix. Similarly, the quantities $\mathscr{K}_{ij}$, $i,j = N, V, M$ in (4) represent dimensional elements of the stiffness matrix of the real system.

2.2. Structure of the macroelement model

A basic remark concerning the formulation of the model is that the global behavior of the system reproduced by the macroelement is actually the result of the combination of soil and soil–footing interface properties. The macroelement should thus reflect rigidity and strength characteristics of the soil as well as strength characteristics of the soil–foundation interface. Different possibilities existing for these properties give rise to different macroelement formulations, for example cohesive soil and perfectly bonded interface, cohesive or frictional soil with frictional interface, *etc.* The macroelement presented herein are developed for applications in earthquake engineering, for which we make the following assumptions:

a. The applied seismic loads being in general of very short duration (of the order of magnitude of a few seconds) in comparison to the characteristic time of water pressure dissipation and assuming a saturated soil, the soil response will correspond to *undrained conditions* of loading. It will be characterized by a Tresca strength criterion with an *associated* plasticity model.

b. The soil–foundation interface is a no-tension interface that allows for uplift of the footing with detachment between the soil and the foundation. This is an essential and desirable feature for applications in earthquake engineering, where it has been commonly observed that such uplift taking place at the foundation level acts as a seismic isolation mechanism for the superstructure [18]. Interface strength criteria that satisfy this condition are the perfectly rough no-tension interface, the Tresca interface without resistance to tension, the Coulomb interface with zero cohesion, *etc.* For the needs of present developments we will retain the perfectly rough no-tension interface.

The soil and the interface strength criteria are combined in the plane directly below the footing and can be represented in a $\sigma-\tau$ diagram, σ denoting the normal and τ the tangential component of the traction on the plane, as in Fig. 4(a). The considered criteria for the soil and the soil–footing interface give rise to a surface of ultimate loads supported by the system that is represented in Fig. 4(b) in the space of the generalized force parameters (Q_N, Q_V, Q_M; *cf.* [19–21]). We insist on the fact that this surface is obtained within the Yield Design framework as a combined result of both soil and the soil–footing interface strength criteria.

Given the aforementioned assumptions for the system behavior, the passage to macroelement is made according to the following modeling principles:

a. The uplift mechanism and the soil plasticity mechanism that govern the system behavior will be modeled independently

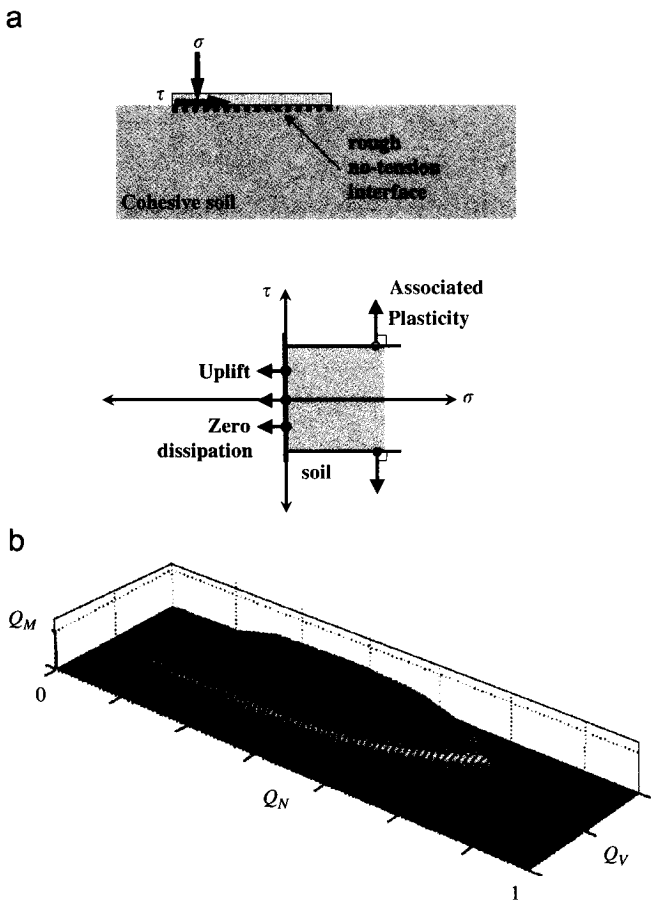

Fig. 4. (a) Assumed behavior at the scale of the constituent materials of the system for a macroelement oriented towards earthquake engineering applications and (b) corresponding surface of ultimate loads of the system in the space (Q_N, Q_V, Q_M).

and incorporated in the macroelement. This will permit retrieval of one mechanism if the other one is deactivated.

b. Fig. 4(a) reveals that the nature of the two mechanisms is completely different. The soil plasticity mechanism is associated with a dissipative process accounting for the irreversible elastoplastic soil behavior. It can be modeled within macroelements by an associated plasticity model formulated in terms of generalized forces and displacements. If we isolate this mechanism by considering that no uplift is allowed at the soil–footing interface, then the obtained global yield surface can be approximated by an ellipsoid centered at the origin in the space of the parameters (Q_N, Q_V, Q_M), as has been shown in [22].

c. The uplift mechanism, pertaining to a non-linearity of geometric nature, is related to a non-dissipative reversible process. Since the construction of macroelements is performed by lumping the entire soil-foundation geometry at a single point, the possibility of modeling the uplift mechanism by continuous updating of the system geometry may seem *a priori* excluded. As a matter of fact, uplift can be modeled within macroelements with a phenomenological non-linear elastic model written in terms of generalized forces and displacements, which respects its reversible and non-dissipative nature and reproduces the apparent reduction of the foundation stiffness or the heave of the footing center as uplift is initiated.

d. The surface of ultimate loads of the system, presented in Fig. 4(b), defines the domain that must strictly contain in its interior all the possible force states that will be obtained by the macroelement model. But there is no reason whatsoever to use the ultimate surface of the system for the definition of the yield surface of the plasticity model. In the examined case, such an assumption cannot be justified since the ultimate surface is obtained as the combined result of both non-linear mechanisms. Let us note that the yield surface of the plasticity model has been traditionally identified with the ultimate surface of the system in the majority of previous macroelement models. Departing from this assumption is an important original feature of the proposed model.

Following the aforementioned remarks, the structure obtained for the macroelement is presented in Fig. 5(a) (plane Q_N–Q_V) and in Fig. 5(b) (plane Q_N–Q_M). The plasticity model is defined by an ellipsoidal yield surface with an associated flow rule and the uplift model by a cut-off at $Q_N = 0$. In the interior of the yield surface, the elastic response of the system remains linear before uplift is initiated and becomes non-linear after uplift initiation. The region $Q_N<0$ corresponds to a situation where the footing is totally detached from the soil and its treatment will not be included in the model.

Concerning the influence of the horizontal force on the uplift model, we will assume, following Crémer [4], that the horizontal force has no effect on the uplift response of the system. This leads to a formulation of the uplift model in terms of the parameters Q_N, Q_M only.

The advantage of the proposed structure is that it can be represented by the very simple rheological model presented in Fig. 6, for which the decomposition of the displacement increment into an elastic (i.e. reversible) and plastic part can be introduced:

$$\dot{\underline{q}} = \dot{\underline{q}}^{el} + \dot{\underline{q}}^{pl} \tag{5}$$

In the following sections we describe in detail the plasticity and uplift models implemented in the macroelement.

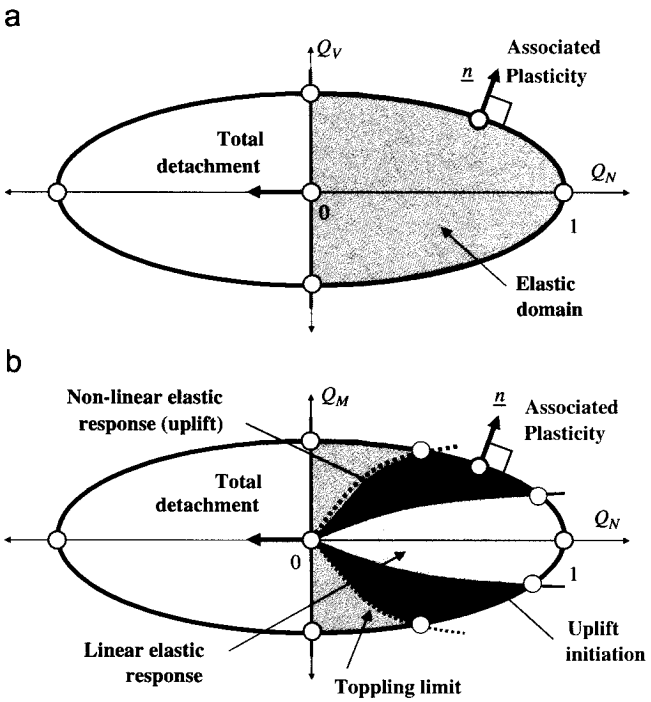

Fig. 5. (a) Structure of the proposed macroelement in the Q_N–Q_V plane and (b) structure of the proposed macroelement in the Q_N–Q_M plane.

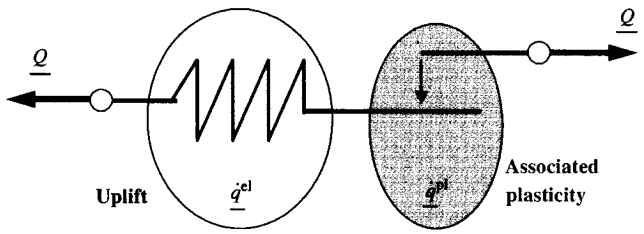

Fig. 6. Rheological model of the proposed macroelement model.

2.3. Non-linear elastic model for uplift

The uplift of the foundation will be described by a phenomenological non-linear elastic model. This permits incorporation of the linear elastic part of the behavior of the system into it. The model will be formulated independently of any plastic soil behavior (we thus consider that the plasticity mechanism is deactivated). We initially introduce an incrementally linear relationship linking the increment of forces with the increment of the elastic displacements:

$$\dot{\underline{Q}} = \underline{\underline{\mathcal{K}}}\,\dot{\underline{q}}^{el} \tag{6}$$

In (6), $\underline{\underline{\mathcal{K}}} = \mathcal{K}_{ij}$, $i, j = N, V, M$ is the tangent elastic stiffness matrix of the system, with elements that are not constant in general. These may be written as functions of the generalized elastic displacements:

$$\mathcal{K}_{ij} = \mathcal{K}_{ij}(\underline{q}^{el}) \tag{7}$$

2.3.1. Elastic stiffness matrix before uplift initiation

Before uplift initiation the system response is linear and the matrix $\underline{\underline{\mathcal{K}}}$ represents elastic impedances of the foundation. For a

footing with planar base that rests on the soil surface the coupling terms are negligible (*cf.* [24]). So the matrix $\underline{\underline{\mathcal{K}}}$ is written as

$$\underline{\underline{\mathcal{K}}} = \begin{bmatrix} \tilde{\mathcal{K}}_{NN} & 0 & 0 \\ 0 & \tilde{\mathcal{K}}_{VV} & 0 \\ 0 & 0 & \tilde{\mathcal{K}}_{MM} \end{bmatrix} \tag{8}$$

In (8), the quantities $\tilde{\mathcal{K}}_{NN}$, $\tilde{\mathcal{K}}_{VV}$, $\tilde{\mathcal{K}}_{MM}$ depend on the foundation geometry and on elastic parameters of the soil.

2.3.2. Elastic stiffness matrix during uplift

The elastic stiffness matrix during uplift has been calibrated using finite-element solutions of a footing uplifting on a purely elastic soil. The model is independent of the horizontal force Q_V and we consider that uplift is initiated when the moment $|Q_M|$ applied on the footing exceeds (in absolute value) a certain value $|Q_{M,0}|$ representing the normalized moment of uplift initiation:

$$\text{Before uplift}: \quad |Q_M| < |Q_{M,0}| \Rightarrow Q_M = \tilde{\mathcal{K}}_{MM} q_M^{el} \tag{9}$$

$$\text{Uplift initiation}: \quad |Q_M| = |Q_{M,0}| \Rightarrow q_{M,0}^{el} = \frac{Q_{M,0}}{\tilde{\mathcal{K}}_{MM}} \tag{10}$$

We note that the quantity $|Q_{M,0}|$ is linear with respect to the vertical force applied on the footing:

$$Q_{M,0} = \pm\frac{Q_N}{\alpha} = \pm\frac{1}{\alpha}\tilde{\mathcal{K}}_{NN} q_N^{el} \tag{11}$$

For strip footings on elastic half-spaces, Crémer [4] and Crémer et al. [5,6] indicate that $\alpha = 4$. For circular footings resting on elastic half-spaces, Wolf [25] indicates that $\alpha = 6$. The elastic angle of rotation at the instant of uplift initiation is written as

$$|q_{M,0}^{el}| = \frac{1}{\tilde{\mathcal{K}}_{MM}}\left(\frac{1}{\alpha}\tilde{\mathcal{K}}_{NN} q_N^{el}\right) \tag{12}$$

For the calibration of the elastic tangent stiffness matrix during uplift we use numerical results presented in [4] for the case of strip footings and [25,26] for the case of circular footings.

Strip footings: The results presented in [4] have been obtained by fixing the applied vertical force on the footing and then increasing the applied moment until toppling of the structure occurs. This means that the increment of the vertical force is zero. So from (6), we can write

$$\dot{Q}_N = \mathcal{K}_{NN}\dot{q}_N + \mathcal{K}_{NM}\dot{q}_M = 0 \tag{13}$$

The increment of the moment is written similarly as

$$\dot{Q}_M = \mathcal{K}_{MN}\dot{q}_N + \mathcal{K}_{MM}\dot{q}_M \tag{14}$$

The two main approximate relations introduced in [4] with respect to the numerical results are the following:

$$\frac{Q_M}{Q_{M,0}} = 2 - \frac{q_{M,0}^{el}}{q_M^{el}} \quad \text{for } |Q_M| > |Q_{M,0}| \tag{15}$$

$$\frac{\dot{q}_N^{el}}{\dot{q}_M^{el}} = -\frac{1}{2}\left(1 - \frac{q_{M,0}^{el}}{q_M^{el}}\right) \tag{16}$$

Expression (15) provides the $Q_M - q_M^{el}$ diagram and expression (16) yields the coupling between the vertical force and the moment during uplift. These two equations are not sufficient for calculation of all the elements of the stiffness matrix. So we will introduce the additional assumption that the element $\mathcal{K}_{NN}$ remains constant during uplift. This means that all the effects of uplift on the vertical force and vertical displacement of the footing will by attributed to the coupling term $\mathcal{K}_{MN} = \mathcal{K}_{NM}$.

The aforementioned assumptions and relations (9)–(16) together with the property of symmetry of $\underline{\underline{\mathcal{K}}}$ lead to the following elastic stiffness matrix:

$$\begin{pmatrix} \dot{Q}_N \\ \dot{Q}_V \\ \dot{Q}_M \end{pmatrix} = \begin{bmatrix} \mathcal{K}_{NN} & 0 & \mathcal{K}_{NM} \\ 0 & \mathcal{K}_{VV} & 0 \\ \mathcal{K}_{MN} & 0 & \mathcal{K}_{MM} \end{bmatrix} \begin{pmatrix} \dot{q}_N^{el} \\ \dot{q}_V^{el} \\ \dot{q}_M^{el} \end{pmatrix} \tag{17}$$

with

$$\mathcal{K}_{NN} = \tilde{\mathcal{K}}_{NN} \tag{18}$$

$$\mathcal{K}_{VV} = \tilde{\mathcal{K}}_{VV} \tag{19}$$

$$\mathcal{K}_{NM} = \mathcal{K}_{MN}\begin{cases} 0 & \text{if } |q_M^{el}| \leqslant |q_{M,0}^{el}| \\ \frac{1}{2}\tilde{\mathcal{K}}_{NN}\left(1 - \dfrac{q_{M,0}^{el}}{q_M^{el}}\right) & \text{if } |q_M^{el}| > |q_{M,0}^{el}| \end{cases} \tag{20}$$

$$\mathcal{K}_{MM} = \begin{cases} \tilde{\mathcal{K}}_{MM} & \text{if } |q_M^{el}| \leqslant |q_{M,0}^{el}| \\ \tilde{\mathcal{K}}_{MM}\left(\dfrac{q_{M,0}^{el}}{q_M^{el}}\right)^2 + \frac{1}{4}\tilde{\mathcal{K}}_{NN}\left(1 - \dfrac{q_{M,0}^{el}}{q_M^{el}}\right)^2 & \text{if } |q_M^{el}| > |q_{M,0}^{el}| \end{cases} \tag{21}$$

The quantity $q_{M,0}^{el}$, which is generally a function of the applied vertical force, is given for an elastic half-space by (12).

Circular footings: By performing similar analyses, Wolf [25] and Wolf and Song [26] obtained results for the case of circular footing uplifting on an elastic half-space. However the results are presented in a different way. The actual irregular contact area has been replaced by an equivalent circle with the same center of gravity. The radius of this equivalent circle is calculated for the two translational degrees of freedom (vertical and horizontal) by equating the real contact area with the area of the equivalent circle. For the rotational degree of freedom, the equivalent radius is calculated by equating the two moments of inertia. Then the elastic stiffness coefficients of the system are calculated using standard formulae for elastic impedances of circular footings ([35] *cf.* Table 2) without the introduction of coupling terms $\mathcal{K}_{ij}$, $i \neq j$. The approximation relationships proposed by Wolf are the following:

$$\begin{cases} Q_{M,0} = \pm\frac{Q_N}{6} \\ \dfrac{D_{N,V}}{D} = -4.296\left(\dfrac{Q_M}{Q_N}\right)^2 - 0.136\left|\dfrac{Q_M}{Q_N}\right| + 1.142 \\ \qquad \text{for } |Q_M| > |Q_{M,0}| \\ \dfrac{D_M}{D} = \frac{3}{2}\left(1 - 2\left|\dfrac{Q_M}{Q_N}\right|\right) \quad \text{for } |Q_M| > |Q_{M,0}| \\ \pm\dfrac{x_S}{D} = \frac{3}{2}\left|\dfrac{Q_M}{Q_N}\right| - \frac{1}{4} \quad \text{for } |Q_M| > |Q_{M,0}| \end{cases} \tag{22}$$

In (22), $D_{N,V}$ and D_M represent the diameter of the equivalent radius for the translational and the rotational degrees of freedom, respectively. Similarly x_S represents the position of the equivalent disk center with respect to the actual center of the footing. This quantity is necessary for the calculation of the vertical displacement of the center of the footing due to uplift. In other words it provides the coupling between the vertical translational and the rotational degree of freedom during uplift.

For the needs of the present formulation, the approximate relationships by Wolf are written in a form similar to the one adopted for strip footings. It can be verified that the relationships (22) are approximately equivalent to the following

Table 2
Summary of model parameters

Numerical parameter	Strip footings	Circular footings	Comments
Normalization procedure			
a	B	D	
N_{max}	$5.14c_0B$	$6.06c_0\pi\frac{D^2}{4}$ (cf. [33])	Homogeneous cohesive soil with cohesion c_0
	cf. the exact solutions of Salençon and Matar		Cohesive soil with linearly varying cohesion. Surcharge and finite soil layer depth taken into account
Linear viscoelastic behavior			
$\tilde{\mathscr{K}}_{NN}$	$\frac{0.73\mathscr{G}}{1-\nu}$	$\frac{2\mathscr{G}D}{1-\nu}$	*cf.* [35]
$\tilde{\mathscr{K}}_{VV}$	$\frac{2\mathscr{G}}{2-\nu}$	$\frac{4\mathscr{G}D}{2-\nu}$	*cf.* [35]
$\tilde{\mathscr{K}}_{MM}$	$\frac{\pi\mathscr{G}}{8(1-\nu)}B^2$	$\frac{\mathscr{G}D^3}{3(1-\nu)}$	*cf.* [35]
C_{NN}	$\rho V_{La}B$	$\rho V_{La}\left(\frac{\pi D^2}{4}\right)$	*cf.* [35], $V_{La}=\frac{3.4}{\pi(1-\nu)}V_S$
C_{VV}	ρV_SB	$\rho V_S\left(\frac{\pi D^2}{4}\right)$	*cf.* [35], $V_S=\sqrt{\frac{\mathscr{G}}{\rho}}$
C_{MM}	$\rho V_{La}\left(\frac{B^2}{12}\right)$	$\rho V_{La}\left(\frac{\pi D^4}{64}\right)$	*cf.* [35], $V_{La}=\frac{3.4}{\pi(1-\nu)}V_S$
Plasticity model			
$Q_{V,max}$	$\frac{c_0B}{N_{max}}\approx 0.2$	$\frac{\pi D^2c_0}{4N_{max}}\approx 0.165$	Footing sliding on a purely cohesive soil
$Q_{M,max}$	$\frac{0.67c_0B^2}{BN_{max}}\approx 0.13$ ([22])	$\frac{0.67c_0AD}{DN_{max}}\approx 0.11$ ([23])	Footing perfectly bonded on a homogeneous cohesive soil
	Use solutions presented in [22]	Use solutions presented in [23]	Footing perfectly bonded on a heterogeneous cohesive soil
h_0	Parameters depending on the particular foundation soil		Calibrated through a loading–unloading–reloading test of the footing under centered vertical force
p_1			
Uplift model			
	$\frac{Q_M}{Q_{M,0}}=2-\frac{q^{el}_{M,0}}{q^{el}_M}$	$\frac{Q_M}{Q_{M,0}}=3-2\left(\frac{q^{el}_{M,0}}{q^{el}_M}\right)^{0.5}$	Approximation relationships used for the calibration of the non-linear elastic stiffness matrix
	$\frac{\dot{q}_N}{\dot{q}_M}=-\frac{1}{2}\left(1-\frac{q^{el}_{M,0}}{q^{el}_M}\right)$	$\frac{\dot{q}_N}{\dot{q}_M}=-\frac{3}{4}\left(1-\frac{q^{el}_{M,0}}{q^{el}_M}\right)$	
$Q_{M,0}$	$\pm\frac{Q_N}{4}\exp(-\beta Q_N)$	$\pm\frac{Q_N}{6}\exp(-\beta Q_N)$	Moment of uplift initiation of footing on elastoplastic soil, $\beta=1.5$–2.5

relationships:

$$\frac{Q_M}{Q_{M,0}}=3-2\left(\frac{q^{el}_{M,0}}{q^{el}_M}\right)^{0.5} \tag{23}$$

$$\frac{\dot{q}^{el}_N}{\dot{q}^{el}_M}=-\frac{3}{4}\left(1-\frac{q^{el}_{M,0}}{q^{el}_M}\right) \tag{24}$$

We proceed thus in a formulation for the elastic stiffness matrix in a way similar to the one adopted for strip footings. From Eqs. (23) and (24) and with the introduction of the same assumption that was adopted for strip footings, the elastic stiffness matrix reads

$$\mathscr{K}_{NN}=\tilde{\mathscr{K}}_{NN} \tag{25}$$

$$\mathscr{K}_{VV}=\tilde{\mathscr{K}}_{VV} \tag{26}$$

$$\mathscr{K}_{NM}=\mathscr{K}_{MN}=\begin{cases}0 & \text{if} \quad |q^{el}_M|\leqslant|q^{el}_{M,0}|\\ \frac{3}{4}\tilde{\mathscr{K}}_{NN}\left(1-\frac{q^{el}_{M,0}}{q^{el}_M}\right) & \text{if} \quad |q^{el}_M|>|q^{el}_{M,0}|\end{cases} \tag{27}$$

$$\mathscr{K}_{MM}=\begin{cases}\tilde{\mathscr{K}}_{MM} & \text{if} \quad |q^{el}_M|\leqslant|q^{el}_{M,0}|\\ \tilde{\mathscr{K}}_{MM}\left(\frac{q^{el}_{M,0}}{q^{el}_M}\right)^{3/2}+\frac{9}{16}\tilde{\mathscr{K}}_{NN}\left(1-\frac{q^{el}_{M,0}}{q^{el}_M}\right)^2 & \text{if} \quad |q^{el}_M|>|q^{el}_{M,0}|\end{cases} \tag{28}$$

2.3.3. Comments

Concerning the formulation of the uplift model the following remarks are worth pointing out:

i. The presented non-linear elastic model for uplift departs from numerical analyses of a footing uplifting on an elastic half-space and ends up (through curve fitting) in some approximate analytical expressions for the elastic stiffness matrix linking the increments of generalized forces and elastic displacements in the system. In performing the passage to macroelements all the information related to the change of the geometry of the contact area is lost and effects of the actual geometric non-linearity are reproduced phenomenologically by a "material-type" non-linearity.
ii. The numerical results used for both strip and circular footings are presented normalized with respect to the vertical force Q_N.

This is admissible because of the assumed linearity of the soil behavior. It also implies that once the stiffness matrix is defined, it can be used for any loading history and not only for load paths of the numerical analyses in [4,25,26].

iii. The available results provide two equations for the four unknown elements of the stiffness matrix. So the solution for the matrix $\underline{\underline{\mathscr{K}}}$ that reproduces the observed behavior cannot be uniquely determined. Besides the presented approach, one has the option of preserving a diagonal matrix even after uplift initiation and then reducing correspondingly the diagonal terms K_{NN}, K_{MM} (as a matter of fact this is Wolf's approach) or even both reducing K_{NN} and K_{MM} and introducing a coupling term K_{NM} simultaneously. Note that a more complete set of results, not yet available, will lead to the exact, unique elastic stiffness matrix of the system.

iv. The criterion of uplift initiation in Eq. (11) should not be confused with the conventional condition of uplift initiation of strip foundations to be smaller than or equal to $B/6$. The former is obtained using the exact normal stress distribution developing below the footing whereas the latter is obtained assuming a linear distribution. We finally note that when the rotation angle q_M^{el} becomes too large we obtain the limits $Q_M \to 2Q_{M,0}$ for strip footings (*cf.* Eq. (15)) and $Q_M \to 3Q_{M,0}$ for circular footings (*cf.* Eq. (23)), which are coherent with standard design rules.

2.4. Plasticity model

For the description of the soil plasticity mechanism we develop a "bounding surface" hypoplastic model following the formulation presented in [27]. This formulation was chosen because: (i) it gives a continuous plastic response even for initial load increments for both virgin loading and reloading, (ii) it is particularly convenient for the description of cyclic behavior and (iii) its simplicity and flexibility are particularly desirable for the numerical treatment of the problem. The principal originality of the model with respect to classical plasticity is the introduction of a surface in the space of generalized forces, called *bounding surface*, allowing for a straightforward and particularly flexible definition of the plastic modulus.

2.4.1. Bounding surface

Following the reasoning of Section 2.2, the bounding surface of the proposed model is identified with an ellipsoid centered at the origin in the space of force parameters. It can thus be described by the equation

$$f_{BS} = (\underline{Q}) = Q_N^2 + \left(\frac{Q_V}{Q_{V,\max}}\right)^2 + \left(\frac{Q_M}{Q_{M,\max}}\right)^2 = 1 \tag{29}$$

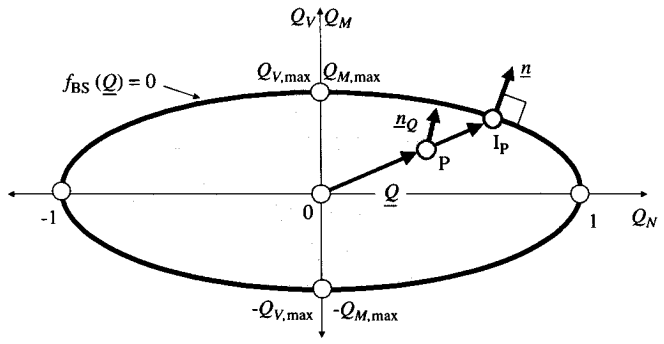

Fig. 7. Bounding surface for the hypoplastic model incorporated in the macro-element.

We note that in the *particular case* where no uplift of the footing is considered, this surface is identified with the surface of ultimate loads of the system and more elaborate approximations can thus be considered. The proposed ellipsoidal bounding surface, while being extremely simple, retains a more than sufficient level of accuracy with respect to the real behavior. The bounding surface is represented in Fig. 7.

The role of the bounding surface is twofold:

a. to define the cases of pure loading, unloading, and neutral loading, and
b. to define the direction of plastic displacement increment and the magnitude of plastic modulus.

In the present hypoplastic formulation, pure loading and reloading are accompanied by the development of plastic displacements whereas in neutral loading and unloading the response is purely elastic.

The objectives (a) and (b) are achieved by introducing a mapping rule, which maps every point in the interior of the bounding surface to a specific point, called *image point*, on the surface boundary. For every point **P** at the interior of the bounding surface we define its corresponding image point using a radial rule as follows (*cf.* Fig. 7):

$$\mathbf{I_P} = \{\lambda \mathbf{P} | \mathbf{I_P} \in \partial f_{BS} \text{ and } \lambda \geqslant 1\} \tag{30}$$

2.4.2. Definition of the plastic modulus

The inverse of the plastic modulus can be written for an associated model in the form

$$\underline{\underline{\mathscr{H}}}^{-1} = \frac{1}{h}(\underline{n} \otimes \underline{n}) \tag{31}$$

In (31), h is a scalar function and $\underline{n}$ is the unit vector normal to the bounding surface on the image point (*cf.* Fig. 7).

The magnitude of the plastic displacement increment is controlled by the scalar quantity h. This quantity is defined as a function of the distance between the current state of forces and its image point. A simple measure of this distance is given by the scalar λ in Eq. (30). We can thus write

$$h = h(\lambda) \tag{32}$$

Eq. (32) can be calibrated using numerical or experimental results. If the loading of the footing under a centered vertical force is considered, a logarithmic variation of the plastic modulus (*cf.* [28]) may be adopted, leading to the particularly simple expression

$$h = h_0 \ln(\lambda) \tag{33}$$

h_0 being a numerical parameter.

A more complicated formulation may be introduced to take into account the history of loading of the system. For example, in [15] the bounding surface evolves following an isotropic hardening rule in pure loading, whereas in unloading/reloading the bounding surface remains fixed and the plastic modulus is defined via the image point of the current state of forces as explained above. In the present formulation, a simpler account of the loading history will be adopted by writing

$$h = h_0 \ln\left[\lambda\left(\frac{\lambda}{\lambda_{\min}}\right)^{p_1}\right] \tag{34}$$

where $\lambda_{\min}$ is the minimum value of λ obtained during loading and p_1 is a numerical parameter expressing the extent of plastic response in reloading. The meaning of (33) and (34) is as follows. For pure loading, $\lambda_{\min} = \lambda$ and we retrieve (33). If λ is large, h is

also large and the magnitude of plastic displacement increment is small. So the response is principally elastic. On the contrary, for λ small, h is also small and the plastic displacement increment is large. In the case where the state of forces reaches the bounding surface, $\lambda \to 1$. Thus $h \to 0$ and the system is led to a state of plastic flow. In the phase of reloading, $\lambda_{\min} > \lambda$ and the response of the system is less plastic than in the phase of initial loading.

The above formulation could be qualified as *isotropic*, in the sense that Eq. (34) remains unaltered for all loading paths. More sophisticated relationships could be introduced if experimental data indicate so, in which the plastic modulus is a function of the distance λ, certain loading history parameters such as $\lambda_{\min}$ and also the loading path.

It is finally noted that the present formulation leads to a response with cycle stabilization for repeated cyclic loading. Shakedown can also be obtained if for instance the parameter p_1 in (34) is allowed to increase as a function of the cumulative dissipated plastic energy during cyclic loading, but this has not yet been included in the model.

2.5. Uplift–plasticity coupling

Up to now the uplift and plasticity mechanisms have been examined separately. In real footing behavior however they appear simultaneously and they are coupled. The coupling between these two mechanisms can be summarized in the following points:

a. *Moment of uplift initiation*: For an elastoplastic soil, vertical stresses below the footing are limited by the soil strength criterion. So the applied moment that is necessary to cause uplift is no longer linear with respect to the vertical force. The relation (12) is thus replaced by an ad hoc approximation relation of the following form, as proposed by Crémer [4]:

$$q_{M,0}^{\mathrm{el}} = \pm \frac{1}{\alpha} \left(\frac{Q_N}{\mathscr{K}_{MM}} \right) \mathrm{e}^{-\beta Q_N} \tag{35}$$

The parameter α is as in (11). The parameter β is a numerical fit parameter that can be investigated by numerical analyses of strip or circular footings uplifting on an elastoplastic soil. For strip footings, Crémer [4] has proposed $\beta = 1.5–2.5$. For circular footings, and in lack of specific experimental and numerical data, β can be calibrated by the condition that force states obtained by macroelements remain within the ultimate surface of the foundation. The range $\beta = 1.5–2.5$ proves to be acceptable.

b. *Direct coupling*: A direct uplift–plasticity coupling is obtained in the first place within the macroelement by observing that both plasticity and uplift mechanisms couple degrees of freedom of the system. If for instance an increment of rotation $\dot{q}_M$ is applied on the footing, this changes both Q_M and Q_N. The change of Q_N leads through (35) to a change of $q_{M,0}^{\mathrm{el}}$ and by consequence to a change of the elastic stiffness matrix $\underline{\underline{\mathscr{K}}}$, which again couples Q_M and Q_N. The formulation is thus highly non-linear and an iterative procedure has to be adopted so that the force state satisfying both mechanisms is determined.

c. *Change of footing contact area*: An even more complicated coupling phenomenon between the two mechanisms is obtained as the footing uplifts and rocks cyclically on an elastoplastic soil. The footing contact area gradually becomes rounded and consequently the characteristic dimension a is reduced. Extremities of the footing remain detached from the soil even in full unloading. This in turn leads to an increase of vertical stresses on the footing and a decrease of $N_{\max}$, which in turn tends to flatten the contact area. The reduction of contact area due to rocking, especially for $q_M > 0.01$ rad, leads to an apparent degradation of rotational stiffness as has been verified experimentally through cyclic tests for both cohesive (*cf.* [29]) and frictional soils (*cf.* [29,31,32]). It follows that the normalization scheme introduced in (1) has to be updated in every load increment according to the irreversible reduction of a and $N_{\max}$. This complicated uplift–plasticity coupling mechanism, which could be qualified as a "second-order phenomenon", has not been included in the presented formulation. In any case, its importance for design purposes is limited since admissible rotations for conventional foundation design would anyway not be larger than 0.01 rad. We note that this limit is more relevant for relatively soft cohesive soils while dense frictional soils may indicate a smaller value. Models addressing this "second-order" effect have been proposed in [30,31].

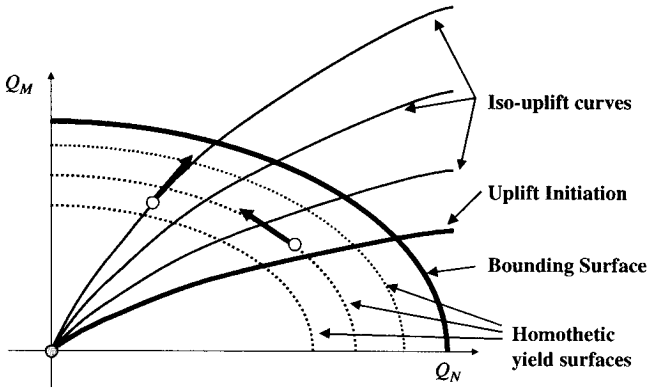

Fig. 8. Neutral loading for plasticity and uplift mechanisms.

d. *Neutral loading*: We may define neutral loading for both mechanisms. As far as the plasticity mechanism is concerned, the hypoplastic bounding surface formulation implies an infinite number of homothetic ellipsoidal yield surfaces. Neutral plastic loading is thus obtained if the force state follows an elliptic path in the space of the loading parameters. For the uplift mechanism, neutral loading may be defined as the combination of moment and vertical loading that is necessary to keep unchanged the detached area of the footing. This has also been considered in [4–6] by the introduction of the so-called "iso-uplift" curves. These are schematically presented together with the homothetic yield surfaces in Fig. 8 in the plane $Q_V = 0$, where it is seen that the two families of curves intersect with one another. So it is not possible to obtain neutral loading for both mechanisms unless the force path follows the intersection of two curves in the three-dimensional space, a rather narrow set of loading paths for real applications.

2.6. Model parameters

In this section, we summarize the parameters of the model and we comment on their determination. These are:

- a: the only geometrical parameter is the footing width B or the footing diameter D, which is prescribed.
- $N_{\max}$: the maximum vertical force supported by the footing in the absence of any horizontal force or moment may be calculated by standard bearing capacity solutions for shallow foundations. In the case of a homogeneous cohesive soil with

cohesion c_0, we obtain

$$N_{max} = 5.14 c_0 B \text{ (strip footings)} \tag{36}$$

$$N_{max} = 6.06 c_0 \frac{\pi D^2}{4} \text{ (circular footings, } cf. \text{ [33])} \tag{37}$$

For soils with linearly varying cohesion, exact bearing capacity solutions presented by Salençon and Matar [34] may be used. They provide the ultimate pressure q_u supported by the soil ($N_{max} = Aq_u$, A: area of footing):

$$q_u = q + \mu_c c_0 \left(N_c + \frac{(\nabla c) a}{4 c_0} \right) \tag{38}$$

$$q_u^\circ = q + \nu_c (q_u - q) \tag{39}$$

In (38) and (39) q_u and q_u° are the ultimate pressure for a strip and a circular footing, respectively, q is the surface surcharge, N_c is a function of a/d where d the depth of the soil layer and μ_c, ν_c are functions of the ratios a/d and $a\ (\nabla c)/c_0$, where ∇c is the vertical cohesion gradient.

- *Elastic foundation impedances*: the commonly used approximate expressions for strip and circular footings on an elastic half-space with constant shear $\mathscr{G}$ and Poisson's ratio ν may be recalled (*cf.* [35]). These have been tabulated in Table 2. Note that the vertical and horizontal elastic impedances of an infinitely long strip footing are actually zero. The proposed values are derived from approximate expressions for rectangular foundations proposed in [35]:

$$\tilde{\mathscr{K}}_{NN} = \frac{\mathscr{G} L}{1-\nu} \left[0.73 + 1.54 \left(\frac{B}{L} \right)^{0.75} \right] \tag{40}$$

$$\tilde{\mathscr{K}}_{VV} = \frac{\mathscr{G} L}{2-\nu} \left[2 + 2.5 \left(\frac{B}{L} \right)^{0.85} \right] \tag{41}$$

where we have let the term on B/L vanish in front of the constant term as $L \to \infty$.

- *Bounding surface*: the parameters defining the bounding surface are
  - o The maximum horizontal force supported by the footing:

$$Q_{V,max} = \frac{V_{max}}{N_{max}} = \frac{c_0 A}{N_{max}} \tag{42}$$

In (42), c_0 designates the soil cohesion at the surface of the soil and A the area of the footing. It is noted that $Q_{V,max}$ is dependent only on the surface cohesion of the soil and not on the vertical cohesion gradient.

  - o The maximum normalized moment $Q_{M,max}$ supported by a footing perfectly bonded on a cohesive soil. For the determination of $Q_{M,max}$ we can use results established in [22] for strip footings and in [23] for circular footings. The aforementioned references cover the case of both homogeneous soils (*cf.* Table 2) and soils with a linearly varying cohesion.
- *Plastic modulus*: the parameters h_0 and p_1 describe the evolution of the magnitude of plastic modulus and may vary significantly for different soil formations. The standard procedure to determine these parameters is a loading–unloading–reloading test of the footing under vertical force only.
- *Surface surcharge, load eccentricity/inclination, embedment depth*: We finally comment on the consideration of foundation configurations with surface surcharge, load eccentricity/inclination and embedment depth. The first can be incorporated into N_{max} as in the solutions by Salençon and Matar [34] (*cf.* Eq. (39)). For the second, it suffices to consider as initial loading conditions (static loading conditions) the combination of Q_N, Q_V, Q_M corresponding to the given load inclination/eccentricity without any modification in the model parameters, (i.e. N_{max} will still refer to the maximum *centered* vertical force). The consideration of the depth of embedment is on the contrary more delicate. For small depths one could possibly adjust the values of N_{max}, $Q_{V,max}$, $Q_{M,max}$ (*cf.* [29] for experimental results) and consider that the non-linear behavior of the system remains otherwise unaffected. However, when the depth of embedment becomes significant, further non-linearities may arise at the lateral footing–soil interfaces pertaining to the behavior of caisson-type foundations. The consideration of a significant depth of embedment is not included in the model.

2.7. Numerical treatment

One of the main concerns regarding the numerical treatment of the macroelement model is that it can be cast into a finite-element code as a separate element. This means that the adopted resolution scheme should be governed by displacements, i.e. given the current state of the system and a total displacement increment, find the decomposition in plastic and elastic components and then update the stresses. This is performed with an iterative algorithm beginning with an elastic prediction. If the prediction violates the bounding surface a "cutting plane"-type algorithm (*cf.* [36]) is implemented in order to bring back the stress state on the bounding surface boundary. If not, an iterative procedure is used to update the elastic and plastic components of the total displacement increments until convergence is achieved. Let us note that, as far as the elastic stiffness matrix is concerned, which also becomes non-linear after uplift initiation, an explicit approximation scheme has been adopted. This proves convenient in terms of incorporation of this additional non-linearity into the plastic model. However, if the iteration step is large, numerical errors in describing uplift behavior of the system may accumulate.

3. Behavior under quasistatic loading

We investigate in this section the system response under quasistatic loading. This is achieved by performing numerical displacement-controlled loading tests. A specific displacement history is prescribed for the footing center and the force–displacement response of the system is computed. Since no strict calibration of the model parameters has been performed, we will limit ourselves to an investigation of qualitative aspects of the system response. Model parameters are presented in Table 3. It will be shown in particular that the surface of ultimate loads of the system, although not explicitly used for the formulation of the two non-linear mechanisms, is nonetheless retrieved as their combined result.

3.1. Vertical force–vertical displacement

We initially examine the system response under a prescribed history of vertical displacement q_N. The results presented in

Table 3
Parameters for the numerical application of Section 3

Numerical parameter	$B = 1$ m, $c_0 = 1$ kPa, $\mathscr{G} = 1000$ kPa, $h_0 = 0.1\tilde{\mathscr{K}}_{NN}$, $p_1 = 5$, $Q_{M,0} = \pm\frac{Q_N}{4}\exp(-1.5Q_N)$, $Q_{V,max} = 0.2$, $Q_{V,max} = 0.13$

Fig. 9(a) provide the model purely elastic and fully elastoplastic response in cycles of loading–unloading and those in Fig. 9(b) present corresponding experimental results obtained in [37]. The bounding surface hypoplastic model predicts a smooth transition towards plastic flow and between the phases of reloading and pure loading. This is a feature that agrees well with the observed soil behavior. We also note that the elastic response of the system (*cf.* Fig. 9(b)) in unloading is almost negligible. This is achieved in the model by prescribing a plastic modulus parameter h_0 considerably smaller than $\mathcal{H}_{NN}$.

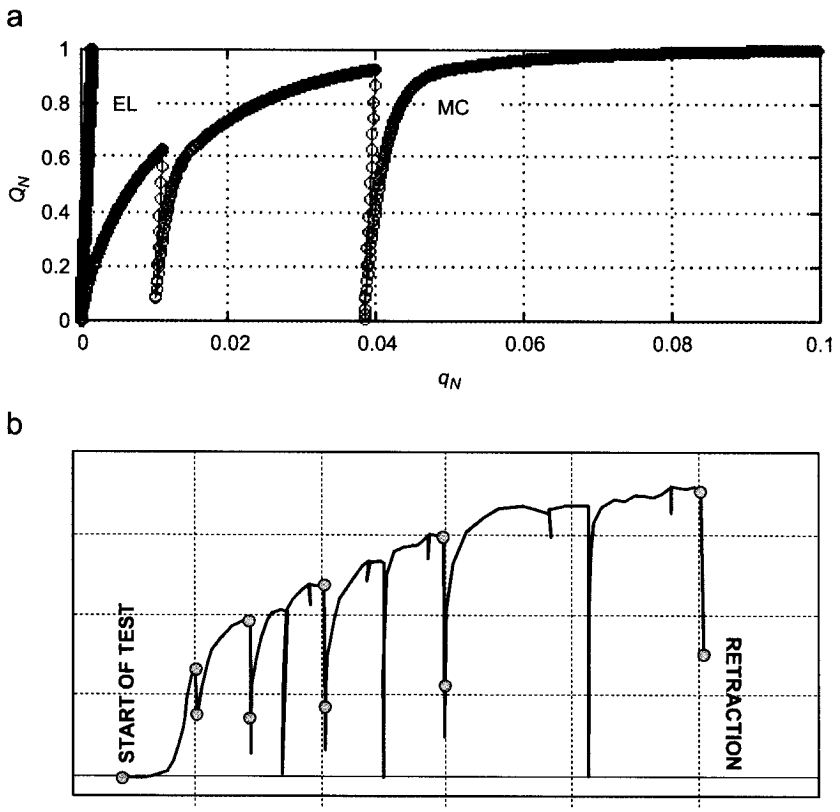

Fig. 9. (a) System response under quasistatic vertical loading and (b) experimental results obtained in [37]. EL, elastic response; MC, full macroelement response.

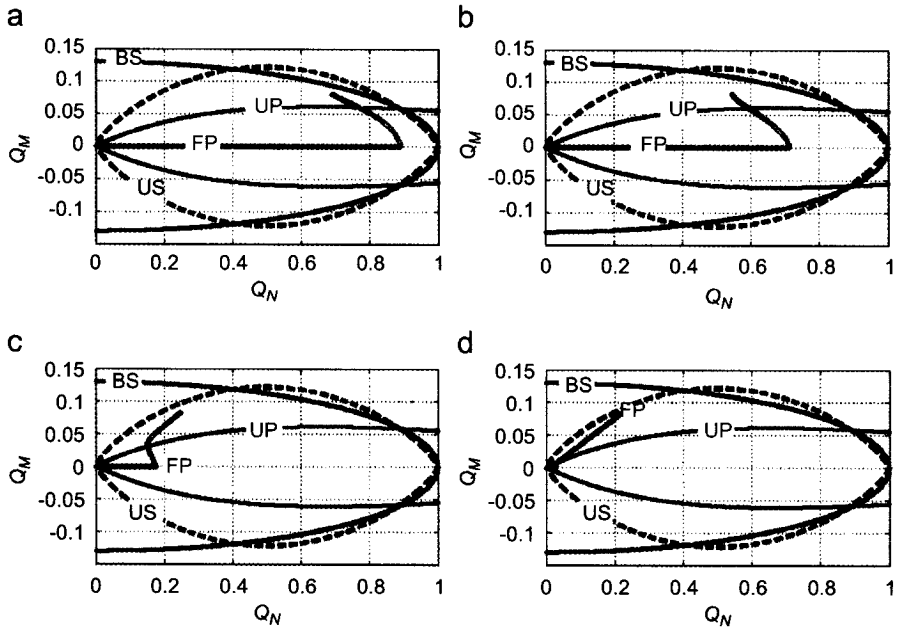

Fig. 10. System response under quasistatic monotonic moment loading. BS, bounding surface; FP, recorded force path; US, ultimate surface; UP, surface of uplift initiation.

3.2. Moment–rotation angle

The response of the system under moment loading is investigated next. Four simulations under monotonic loading are presented in Fig. 10. In these tests, the following displacement histories are applied:

(a) vertical displacement $q_N = 0.1$, then rotation angle $q_M = 0.01$;
(b) vertical displacement $q_N = 0.05$, then rotation angle $q_M = 0.01$;
(c) vertical displacement $q_N = 0.005$, then rotation angle $q_M = 0.01$ and
(d) vertical displacement $q_N = 0.0005$, then rotation angle $q_M = 0.01$.

For every simulation, we present the trace of the vector $\underline{Q}$ in the space of generalized forces (plane Q_M–Q_N). Each diagram contains three additional curves: the elliptical bounding surface, the curve representing the moment of uplift initiation $Q_{M,0}$ as a function of Q_N and finally the surface of ultimate loads of the system (rugby-ball-shaped curve). The curve of uplift initiation is given by the expression as in [5,6]:

$$Q_{M,0} = \pm\frac{Q_N}{4}\exp(-1.5Q_N) \tag{43}$$

The surface of ultimate loads has been found to be sufficiently approximated by the expression proposed in [5,6], which is the one adopted herein:

$$Q_M = \pm 0.37 Q_N^{0.8}(1 - Q_N)^{0.8} \tag{44}$$

The results reveal how mechanisms of plasticity and uplift are combined to provide admissible states of forces of the system. As is seen, these prove to be always included in the interior of the surface of ultimate loads. As the initial vertical displacement becomes smaller and smaller the effect of the plasticity mechanism gradually decreases. In parallel, the effect of uplift becomes more and more important and, once the uplift initiation curve is crossed, a shift is induced in the direction of the force trajectory. The force path in diagram (d) is almost linear with a slope approximately equal to 1/3: this is linked to the standard bearing capacity restriction for strip and rectangular footings that the eccentricity (expressed herein by the ratio Q_M/Q_N) should be less than 1/3. Actually this condition is slightly more conservative than the "exact" force path, showing its perfect compliance with the presented results. The results also show that although the surface of ultimate loads is not explicitly used in the formulation of either the plasticity or the uplift model, it is possible to formulate both models independently (respecting their particular characteristics), but in such a way that the obtained force states are always contained in the interior of the surface of ultimate loads of the system.

4. Extension to dynamic loading

The structure of the macroelement model presented so far refers to the system behavior under quasistatic monotonic or cyclic loading (terms in the equilibrium equations associated with acceleration and velocity have been neglected). However, the principal domain of application for macroelements is using them for efficient non-linear dynamic soil–structure interaction analyses. In this paragraph, we explain under which assumptions the macroelement is incorporated into the global superstructure model and we present, in a numerical application of the dynamic analysis of a real structure, the type of results that can be obtained with the macroelement.

4.1. General principles

The extension of the domain of application of the macroelement to dynamic loading conditions is performed by considering that the soil domain is divided into two separate sub-domains: the near field and the far field. The near field is identified as the soil sub-domain in the footing vicinity where all the non-linearities (material and geometric) of the system take place. These are described within the macroelement by the plasticity and the uplift model as has been explained. The far field, on the other hand, is the soil sub-domain where the response remains purely linear. This distinction between near and far fields permits description of the contribution of far field on the system behavior using dynamic (elastic) impedances of the foundation and the contribution of the near field with macroelements. Extension to dynamic loading conditions may thus be achieved by performing the following:

a. Identifying the parameters $\tilde{K}_{NN}, \tilde{K}_{VV}, \tilde{K}_{MM}$ in the uplift non-linear elastic model of macroelements as the real part of the corresponding dynamic impedances of the footing.
b. Introducing the imaginary part of the retained dynamic impedances in order to account for the phenomenon of radiation damping.
c. Resolution of the system is performed in the time domain and no dependence of dynamic impedances on the frequency of excitation is considered. The retained dynamic impedances can thus correspond (as done in engineering practice) to some characteristic frequency of the system, such as its fundamental eigen-frequency, *etc.*
d. Material damping in the near field is directly reproduced by the plasticity model of macroelements.

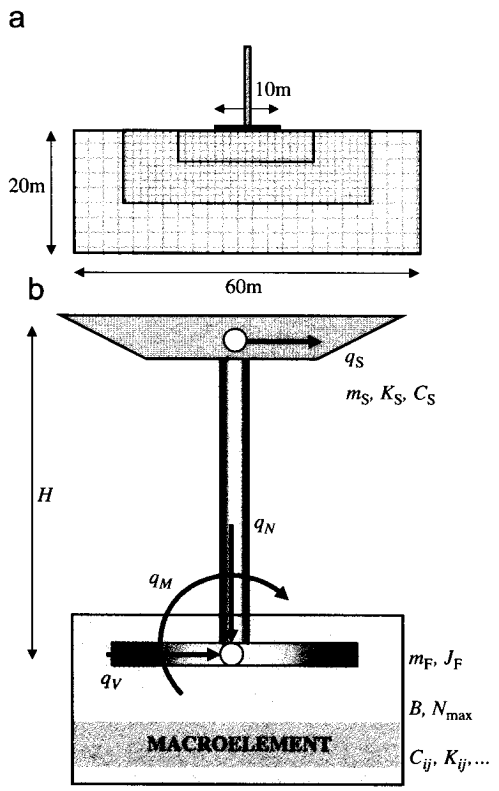

Fig. 11. (a) Finite-element mesh for numerical application (*cf.* [6]) and (b) simple model for dynamic analysis with macroelements.

Table 4
Parameters for the numerical application of Section 4.2

Numerical parameter	DYNAFLOW with soil mesh ([6])	Macroelement
Structure	$m_S = 5 \times 10^4$ kg; $J_S = 1.25 \times 10^6$ kg m^2; $H = 20$ m; $S = 1.6$ m^2 $I = 2.13$ m^4; $E = 35 \times 10^9$ Pa	
Foundation	$B = 10$ m; $e = 0.7$ m; $L = 1.0$ m; $\rho = 18 \times 10^3$ kg/m^3; $E \to \infty$	$B = 10$ m; $m_F = 12 \times 10^3$ kg $J_F = 1.0 \times 10^5$ kg m^2; $N_{max} = 2.4 \times 10^6$ N
Interface	Uplift allowed; no sliding	$\tilde{\mathcal{K}}_{NN} = 2.3 \times 10^8$ N/m $\tilde{\mathcal{K}}_{VV} = 1.1 \times 10^8$ N/m
Soil	$c = c_0 + 3z$ (c, c_0 in kPa, z in m) $c_0 = 30$ kPa $\mathcal{G}/c = 1300$; $\nu = 0.48$ $\rho = 19 \times 10^3$ (kg/m^3)+plastic parameters of the multi-yield law	$\tilde{\mathcal{K}}_{MM} = 3.7 \times 10^9$ N m/rad $C_{NN} = 5.3 \times 10^6$ N s/m $C_{VV} = 2.7 \times 10^6$ N s/m $C_{MM} = 4.4 \times 10^7$ N m s/rad $Q_{V,max} = 0.2$ $Q_{V,max} = 0.13$ $Q_{M,0} = \pm\frac{Q_N}{4}\exp(-2.5Q_N)$ $h_0 = 0.1\tilde{\mathcal{K}}_{NN}$; $p_1 = 5$

Units are considered per unit length of the strip footing.

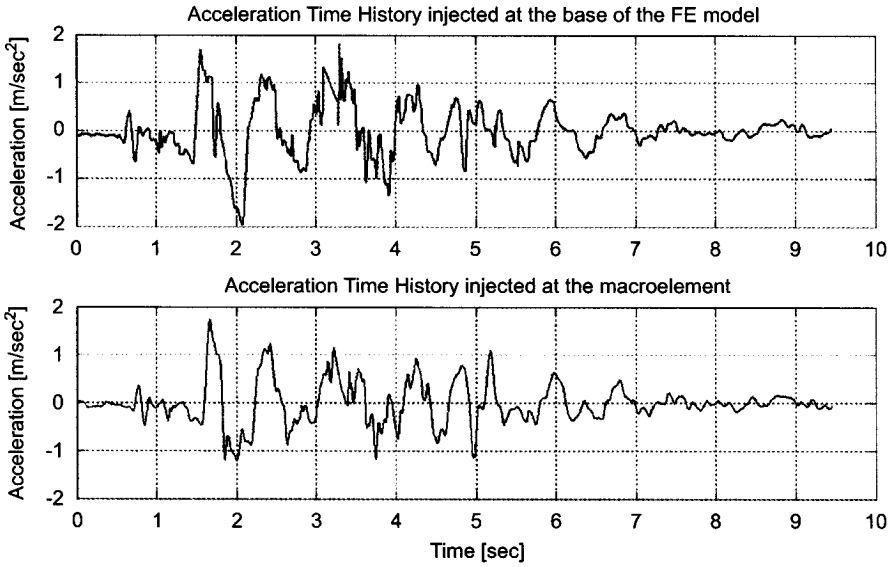

Fig. 12. Acceleration time histories used in the numerical application.

4.2. Numerical application

In order to illustrate the results that can be obtained using the macroelement we present an example of application of the proposed model for the dynamic analysis of a bridge column subjected to a real seismic acceleration time history. The examined structure is modeled with a simple structural model as the one presented in Fig. 11(b). The model exhibits four degrees of freedom: the horizontal translation of the deck and the horizontal and vertical translations and the rotation of the column foundation. The latter three will be described by the macroelement. The results of our analysis are compared with results obtained in [4,6] using a more sophisticated model of the examined system. Soil is modeled with a fine mesh of finite elements (*cf.* Fig. 11(a)); its constitutive model is the multi-yield constitutive law presented in [39]. A complete description of the finite-element model (FEM) model is given in [4,6]. The model was analyzed with the code DYNAFLOW (*cf.* [40]). Numerical parameters for the FEM and the application with the macroelement are summarized in Table 4.

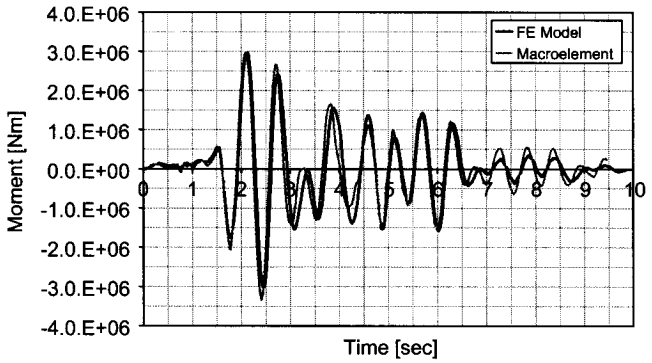

Fig. 13. Response of the system considering purely linear behavior.

The system is subjected to the acceleration time history recorded in the Gemona station during the Friuli earthquake (Italy, 1976) scaled at 0.2g, which is represented in Fig. 12. This accelerogram is injected at the base of the FEM. The acceleration

time history used in the macroelement model is the one computed at the surface-free field in the FEM. No vertical input motion component has been considered. Integration of the equilibrium equation has been performed using a Newmark-type integration scheme. In the following, we present the results of the dynamic analysis for the cases of:

a. linear elastic behavior (uplift and plasticity mechanisms deactivated) and
b. full elastoplastic behavior with uplift.

4.2.1. Linear elastic behavior

A preliminary elastic analysis has been performed in order to check the compatibility of the two acceleration time histories and the elastic parameters of the macroelement model. The evolution of the moment on the foundation with time is represented for the two models in Fig. 13. The macroelement reproduces very well the purely elastic response of the system both in terms of frequencies and in terms of moment amplitudes. The maximum moment on the footing is around $\max M \approx 3.3$ MN m.

4.2.2. Elastoplastic behavior with uplift

Fig. 14 presents four diagrams related to the behavior of the system with the two non-linear mechanisms of uplift and soil plasticization activated. In particular, the following diagrams are presented:

a. the moment–rotation angle diagram for the case of purely elastic response and elastoplastic response with uplift,
b. the evolution of the moment on the foundation,
c. the evolution of the rocking angle of the foundation and
d. the evolution of vertical displacement of the foundation.

The last three diagrams contain the curves obtained with both the macroelement and the FEM. The following remarks may be made:

- The moment–rotation diagram reveals how the two mechanisms are combined. One part of the response remains reversible because of uplift but now we also have the creation of cycles of energy dissipation during loading.
- The activation of the two non-linear mechanisms leads to a significant isolation effect on the foundation. The maximum

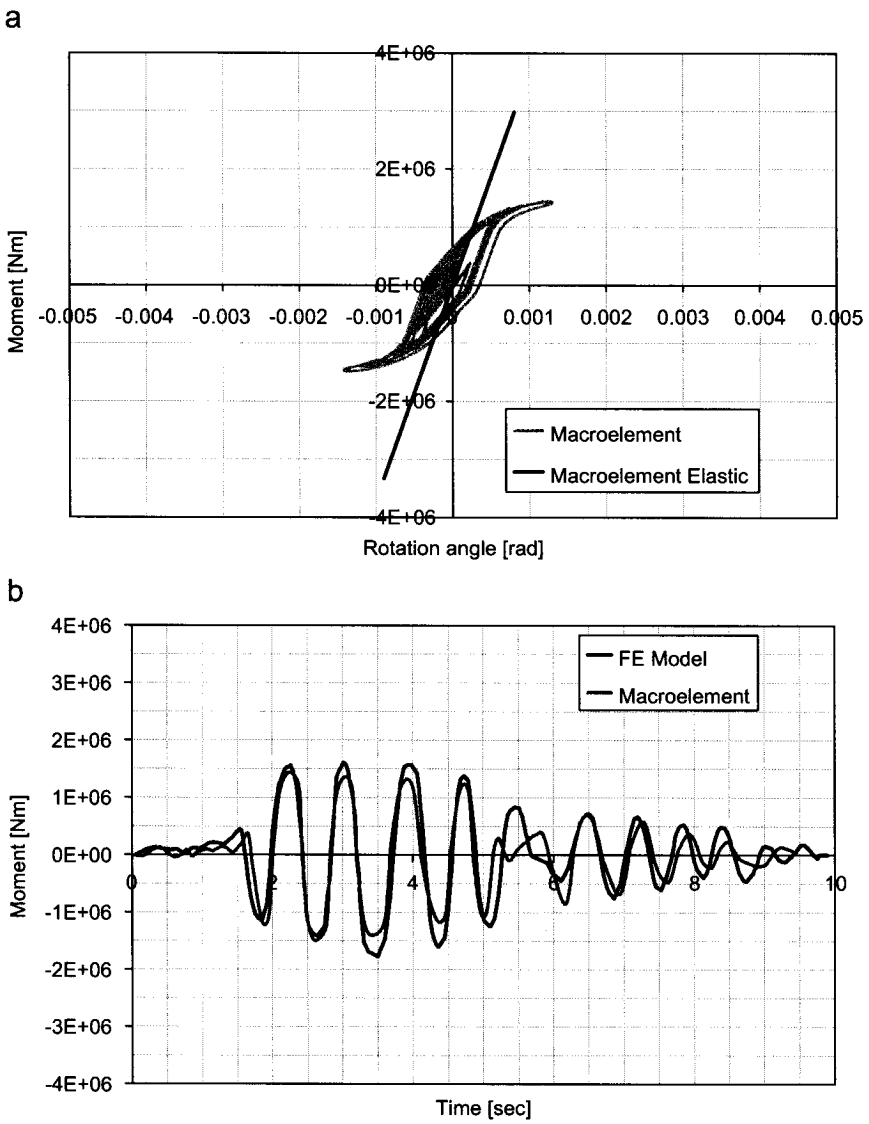

Fig. 14. System response considering full elastoplastic behavior with uplift.

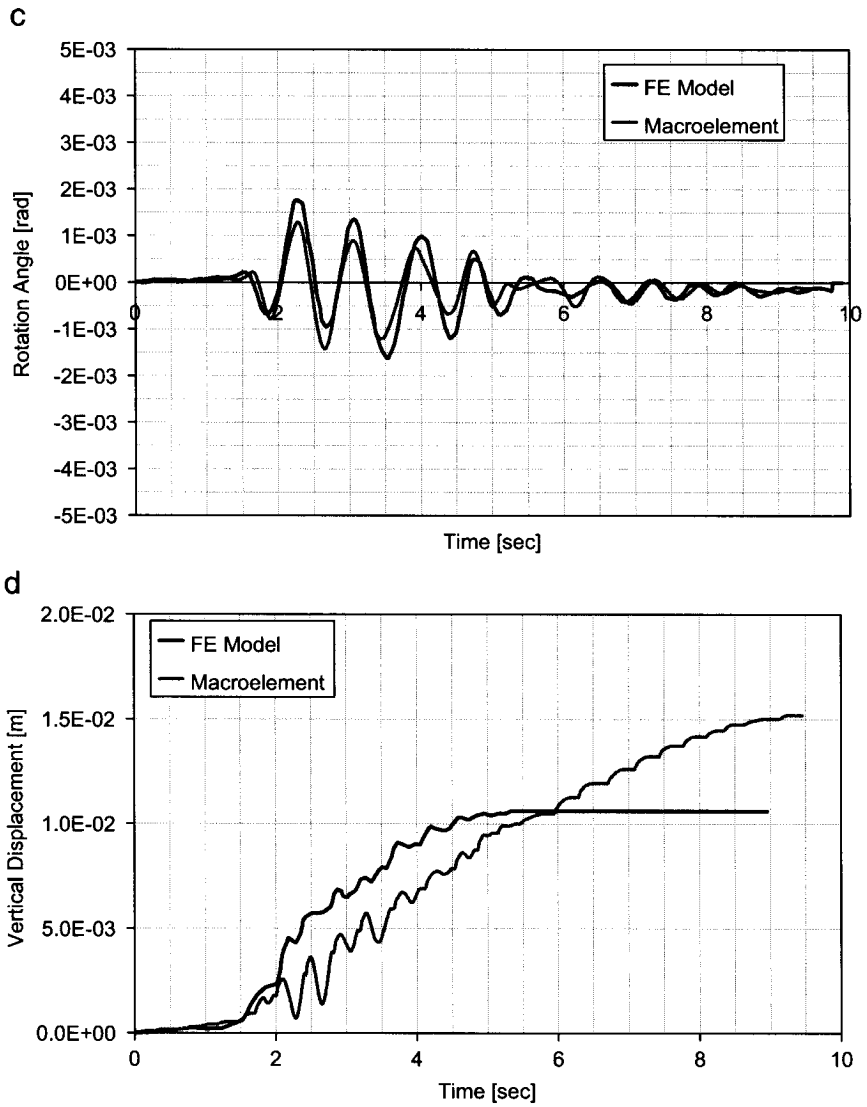

Fig. 14. (*Continued*)

moment on the footing does not exceed the value of 1.8 MN m. The rotation angle remains less than 0.002 rad. One can also observe a small residual rotation accumulated at the end of the excitation. The vertical displacement of the foundation is however rather significant, reaching the value of 0.01 m. The results emphasize the gain but also the price to pay in considering non-linear effects in foundation design: forces are reduced substantially, leading to a far more profitable design. Nevertheless, the maximum and residual displacements have to remain below certain performance limits.

- The macroelement reproduces very well the evolution of the moment and the rotation angle on the foundation. They also provide a satisfactory estimate of the residual vertical displacement of the footing (settlement is denoted as positive). Actually, the observed difference may be attributed to the fact that the plasticity model in the macroelement leads to cycle stabilization in repeated loading (the vertical settlement thus continuously increases throughout the loading). On the other hand, the plasticity formulation in the FEM leads to shakedown. The vertical settlement ceases to increase after approximately half the duration of the excitation.

5. Conclusions

The macroelement model presented in this paper incorporates an associated plasticity model that can account for the soil elastoplastic response in undrained conditions and a phenomenological non-linear elastic model for the uplift mechanism. It was shown that these two mechanisms may be formulated independently from one another and then combined in such a way so that the obtained force states are contained in the interior of the surface of ultimate loads of the system, attributing to this surface its real meaning from the point of view of Yield Design theory (*cf.* [38]), i.e. domain of all the combinations of loads that can be supported by the system.

From the point of view of its numerical treatment, the proposed formulation reduces to a particularly simple rheological model and allows for a simultaneous resolution of both mechanisms. It is particularly flexible in modifying, activating or deactivating different mechanisms, since the modeling of each mechanism is performed independently. Moreover, its extension to fully three-dimensional configurations is straightforward, especially as regards the uplift model that is written with respect

to generalized displacement parameters without introduction of additional parameters linked with the footing geometry.

The proposed model offers a simple and attractive framework, the validity of which was illustrated through a number of theoretical examples.

The model up to its present state of development is nevertheless bound to have certain limitations. These may be summarized in the following points:

a. There is the need for an extensive validation procedure and calibration of numerical parameters, especially for the plasticity model. This procedure would eventually lead to a classification of soils and a set of parameters associated to each class, also comprising qualitative characteristics of the response (*e.g.* shakedown, cycle stabilization, *etc.*)
b. In terms of algorithmic aspects, an implicit resolution scheme for the uplift non-linear elastic model would further increase the accuracy of the model.
c. The dependence of foundation impedances on frequency of excitation has not been taken into account and constant dynamic impedances have been used. A topic for future research could be to incorporate simple models for frequency-dependent impedances as in [41] within macroelements.
d. The introduction of effects of the seismic acceleration on the bearing capacity of the foundation would give further insight to earthquake engineering applications. This has been the subject of recent work by the authors (*cf.* [21]) and it can be performed by introducing the variation of N_{max} due to the incident acceleration in each time step.
e. An extension of the model to the case of a frictional material obeying the Mohr–Coulomb strength criterion is also essential. This would require the introduction of a sliding mechanism along the interface and the formulation of a non-associated plasticity model.
f. The introduction in the model of "second-order effects" such as the reduction of contact area due to rounding of the soil surface when both uplift and soil yielding occur, the gradual settlement of the footing inducing a "depth of embedment" effect, the consequent variation of N_{max} due to these effects, *etc.* are also essential for the validation of the model. Actually, it is deemed that displacement levels beyond which these phenomena become important could serve as limits for a "performance-based" design of shallow foundations.

Acknowledgments

The first author wishes to thank the École Polytechnique and the Public Benefit Foundation "Alexandros S. Onassis" for the financial support during the execution of this study. The authors would also like to thank the reviewers of this paper for their fruitful comments.

References

[1] Nova R, Montrasio L. Settlements of shallow foundations on sand. Géotechnique 1999;41(2):243–56.
[2] Paolucci R. Simplified evaluation of earthquake-induced permanent displacements of shallow foundations. J Earthquake Eng 1997;1(3):563–79.
[3] Pedretti S. Non linear seismic soil foundation interaction: analysis and modelling method. PhD thesis, Dpt Ing Strutturale, Politecnico di Milano, 1998.
[4] Crémer C. Modélisation du comportement non linéaire des fondations superficielles sous séisme. PhD thesis, Laboratoire de Mécanique et de Technologie, ENS—Cachan, France, 2001.
[5] Crémer C, Pecker A, Davenne L. Cyclic macro-element for soil–structure interaction: material and geometrical non linearities. Int J Num Anal Methods Geomech 2001;25:1257–84.
[6] Crémer C, Pecker A, Davenne L. Modelling of nonlinear dynamic behavior of a shallow strip foundation with macroelement. J Earthquake Eng 2002;6(2): 175–211.
[7] Le Pape Y, Sieffert JG, Harlicot P. Analyse non linéaire par macro-éléments du comportement des fondations superficielles sous action sismique. In: Comptes Rendus du 5ème Colloque National AFPS, Cachan, France, 19–21 Octobre 1999, p. 207–14.
[8] Le Pape Y, Sieffert JG. Application of thermodynamics to the global modelling of shallow foundations on frictional material. Int J Num Anal Methods Geomech 2001;25:1140–377.
[9] Houlsby GT, Cassidy MJ, Einav I. A generalised Winkler model for the behaviour of shallow foundations. Géotechnique 2005;55(6):449–60.
[10] Einav I, Cassidy MJ. A framework for modelling rigid footing behaviour based on energy principles. Comput Geotech 2005;32:491–504.
[11] Wood DM, Kalasin T. Macroelement for study of the dynamic response of gravity retaining walls. In: Triandafyllidis N, editor. Cyclic behaviour of soils and liquefaction phenomena. London: Taylor & Francis; 2004. p. 551–61.
[12] Gottardi G, Houlsby GT, Butterfield R. Plastic response of circular footings on sand under general planar loading. Géotechnique 1999;49(4):453–69.
[13] Martin CM, Houlsby GT. Combined loading of spudcan foundations on clay: laboratory tests. Géotechnique 2000;50(4):325–38.
[14] Houlsby GT, Cassidy MJ. A plasticity model for the behaviour of footings on sand under combined loading. Géotechnique 2002;52(2):117–29.
[15] Di Prisco C, Nova R, Sibilia A. Shallow footing under cyclic loading: experimental behavior and constitutive modeling. In: Maugeri M, Nova R, editors. Geotechnical analysis of the seismic vulnerability of historical monuments. Pàtron; 2003. p. 99–121.
[16] Cassidy MJ, Martin CM, Houlsby GT. Development and application of force resultant models describing jack-up foundation behaviour. Mar Struct 2004; 17:165–93.
[17] Grange S, Kotronis P, Mazars J. Advancement of simplified modeling strategies for 3D phenomena and or/boundary conditions for base-isolated buildings or specific soil–structure interactions. Deliverable report 67, Risk mitigation for earthquakes and landslides integrated project, European Program LESSLOSS, September 2006.
[18] Psycharis IN. Dynamic behavior of rocking structures allowed to uplift. J Earthquake Eng Struct Dyn 1983;11:57–76;
Psycharis IN. Dynamic behavior of rocking structures allowed to uplift. J Earthquake Eng Struct Dyn 1983;11:501–21.
[19] Salençon J, Pecker A. Ultimate bearing capacity of shallow foundations under inclined and eccentric loads. Part I: purely cohesive soil. Eur J Mech 1995; 14(3):349–75.
[20] Salençon J, Pecker A. Ultimate bearing capacity of shallow foundations under inclined and eccentric loads. Part II: purely cohesive soil without tensile strength. Eur J Mech 1995;14(3):377–96.
[21] Chatzigogos CT, Pecker A, Salençon J. Seismic bearing capacity of a circular footing on a heterogeneous cohesive soil. Soils Found 2007;47(4):783–97.
[22] Bransby MF, Randolph MF. Combined loading of skirted foundations. Géotechnique 1998;48(5):637–55.
[23] Randolph MF, Puzrin AM. Upper-bound limit analysis of circular foundations on clay under general loading. Geotechnique 2003;53(9):785–96.
[24] Veletsos AS, Wei YT. Lateral and rocking vibrations of footings. ASCE J Soil Mech Found Div 2001;97(9):1227–48.
[25] Wolf JP. Soil–structure interaction analysis in the time domain. New Jersey: Prentice-Hall; 1988.
[26] Wolf JP, Song C. Some cornerstones of dynamic soil–structure interaction. Eng Struct 2002;24:13–28.
[27] Dafalias YF, Hermann LR. Bounding surface formulation of soil plasticity. In: Pande GN, Zienkiewicz OC, editors. Soil mechanics—transient and cyclic loading. New York: Wiley; 1982. p. 173–218.
[28] Butterfield R. A simple analysis of the load capacity of rigid footings on granular materials. J Géotech 1980:128–34.
[29] Gajan S, Kutter BL, Phalen JD, Hutchinson TC, Martic GR. Centrifuge modeling of load–deformation behavior of rocking shallow foundations. Soil Dyn Earthquake Eng 2005;25:773–83.
[30] Gajan S, Kutter BL. A contact interface model for non-linear cyclic moment–rotation behaviour of shallow foundations. In: Proceedings of the fourth international conference on earthquake geotechnical engineering, paper no. 1458, Thessaloniki, Greece, 25–28 June 2007.
[31] Paolucci R, Shirato M, Yilmaz MT. Seismic behaviour of shallow foundations: shaking table experiments vs. numerical modelling. Earthquake Eng Struct Dyn 2007.
[32] Faccioli E, Paolucci R, Vivero G. Investigation of seismic soil–footing interaction by large scale cyclic tests and analytical models. In: Proceedings of the fourth international conference on recent advances in geotechnical earthquake engineering and soil dynamics, March 26–31 2001, San Diego, CA, USA.
[33] Eason G, Shield RT. The plastic indentation of a semi-infinite solid by a perfectly rough circular punch. J Appl Math Phys (ZAMP) 1960;11(1): 33–43.
[34] Salençon J, Matar M. Capacité portante des fondations superficielles circulaires. J Méc Théor Appl 1982;1(2):237–67.
[35] Gazetas G. Foundations vibrations. In: Fang HY, editor. Foundation engineering handbook. New York: van Nostrand Reinhold; 1991 [Chapter 15].
[36] Simo JC, Hughes TJR. Computational inelasticity. New York: Springer; 1998.
[37] Martin CM, Houlsby GT. Combined loading of spudcan foundations on clay: numerical modeling. Géotechnique 2001;51(8):687–99.

[38] Salençon J. An introduction to the yield design theory and its applications in soil mechanics. Eur J Mech A Solids 1990;9(5):477–500.
[39] Prévost JH. Anisotropic undrained stress–strain behaviour of clays. J Geotech Eng Div ASCE 1978;8:1075–90.
[40] Prévost JH. DYNAFLOW: a finite element analysis program for static and transient response of linear and non-linear two and three-dimensional systems. User manual. Princeton, NJ: Department of Civil Engineering, Princeton University; 1999.
[41] Saitoh M. A simple model of frequency-dependent impedance functions in soil–structure interaction using frequency independent elements. J Eng Mech ASCE 2007;133(10):1101–14.